Bulletin of Electrical Engineering and Informatics
Vol. 15, No. 4, August 2026, pp. 3047~3057
ISSN: 2302-9285, DOI: 10.11591/eei.v15i4.11426

A new compact printed ring bandpass filter structure for ISM band applications

Soufiane El Maimouni[1], Fouad Aytouna[1,2], Jamal Zbitou[1,2], Stéphane Ginestar[3], Mohammed El Gibari[3]
[1]Laboratory of Information and Communication Technologies, National School of Applied Sciences of Tangier (ENSAT), Abdelmalek Essaâdi University, Tangier, Morocco
[2]National School of Applied Sciences of Tetouan (ENSATe), Abdelmalek Essaâdi University, Tetouan, Morocco
[3]Centre National de la Recherche Scientifique (CNRS), Institut d'Électronique et des Technologies du Numérique (IETR), Nantes Université, Nantes, France

Article Info

Article history:

Received Sep 21, 2025
Revised Apr 10, 2026
Accepted Jul 9, 2026

Keywords:

Bandpass filter
Coupled ring
Energy harvesting
ISM band
Microstrip technology

ABSTRACT

We introduce a novel, compact bandpass filter (BPF) that employs Ring coupling through a microstrip design. This filter features a ring resonator that mainly relies on capacitive coupling to achieve its resonant characteristic. The results from experimental fabrication confirmed the expected performance of the filter, showing strong agreement between the simulated and measured S-parameters. The filter is built on a RO4003C substrate that is 1.52 mm thick, with a dielectric constant of 3.38 and a loss tangent of 0.0027. Designed for a center frequency of 5.72 GHz and a bandwidth of 930 MHz, it exhibits low insertion loss and effective signal rejection, as supported by advanced electromagnetic simulations. This flexible and efficient filter design represents a significant step forward, offering great potential for innovative communication systems and wireless power transmission, especially when integrated with 5.8 GHz straight-through antenna arrays for wireless energy harvesting.

Corresponding Author:

Soufiane El Maimouni
Laboratory of Information and Communication Technologies
National School of Applied Sciences of Tangier (ENSAT), Abdelmalek Essaâdi University
Tangier, Morocco
Email: soufiane.elmaimouni@etu.uae.ac.ma

1. INTRODUCTION

As the demand for faster data transmission and improved mobility increases, the evolution of wireless communication technologies is accelerating. Since numerous wireless signals operate within the same frequency spectrum, it is essential for communication devices to effectively filter and distinguish these signals to function correctly. This is where band-pass filters become important. They play a vital role for both transmitters and receivers by allowing only the desired frequencies to pass through while blocking unwanted interference, thereby facilitating clear and efficient communication [1]-[8]. Due to its planar design, high reproducibility, and lower sensitivity to manufacturing inconsistencies, microstrip technology has emerged as a preferred method for developing filters in communication systems [9]-[13]. Microstrip ring resonators are often selected for producing effective band-pass filters due to their ability to create filters that are selective, compact, and cost-efficient. These filters find applications in various communication and signal processing systems, prompting engineers to investigate numerous configurations of ring resonators [14]-[17]. Metamaterials, which are artificial structures characterized by unique attributes such as negative permittivity and permeability, have led to significant advancements in radio frequency (RF) filtering. This progress can be traced back to important developments, including Vassalage's theoretical contributions in 1968 and Pendry's introduction of the split-ring resonator in 1999 [2]-[23]. As illustrated in Figure 1, a rectenna system employs bandpass filters to effectively convert electromagnetic energy into electrical energy. These filters are crucial for ensuring impedance matching and minimizing interference, both of which are essential for efficient energy conversion [24].

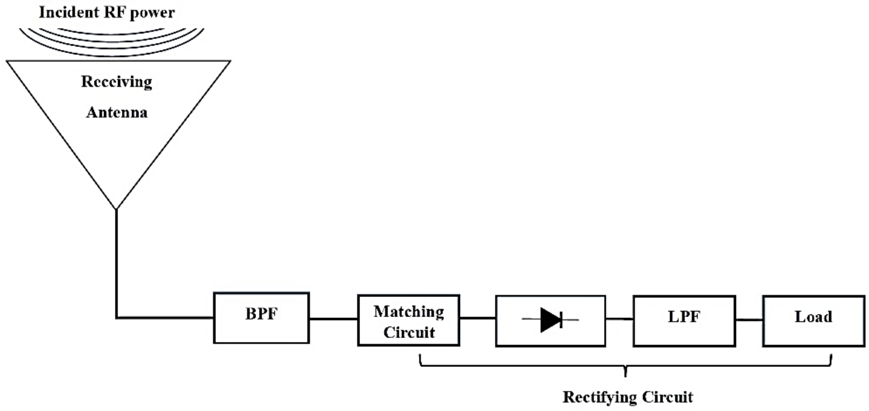

Figure 1. The block diagram of a rectenna system [24]

A rectenna system operates through a series of stages. Initially, an antenna, specifically selected for a certain frequency, captures surrounding radio waves and transforms them into an alternating current (AC) electrical signal. Following this, a bandpass filter (BPF) isolates a particular frequency range, which is vital for enhancing the efficiency of energy collection. To facilitate optimal power transfer, an impedance matching network links the antenna to the rectifier. The rectifier, which typically employs low voltage Schottky diodes, converts the AC signal into a pulsed direct current (DC) signal. A low-pass filter then eliminates the fluctuations in this signal, resulting in a steady DC voltage. Ultimately, this energy is directed to a DC load, such as a battery or supercapacitor, for storage. Numerous band-pass filters utilizing circular ring resonators have been documented in existing literature [24]. However, many of these designs are hindered by relatively large sizes or insufficient stop-band rejection. Furthermore, achieving effective miniaturization while ensuring low insertion loss and adequate selectivity continues to be a significant challenge, particularly for systems functioning within the 5.8 GHz ISM band and energy-harvesting applications.

To address these challenges, this study presents a compact microstrip bandpass filter featuring a novel coupled ring structure. The primary innovation of this design lies in the optimization of electromagnetic coupling paired with the incorporation of perturbation stubs, which enhance selectivity and improve harmonic suppression. Unlike many earlier works that primarily focus on simulation outcomes, the proposed filter has been fabricated and subjected to experimental validation. The results obtained from measurements align closely with the simulations, indicating that the design is both reliable and appropriate for applications within the 5.8 GHz ISM band and energy-harvesting systems.

The main objective of this research is to create an innovative, compact ring annular BPF. We attained optimal performance including the desired return loss, excellent insertion loss, and a reduced size by meticulously adjusting and refining key parameters through two separate electromagnetic simulations. The effectiveness of the filter was subsequently confirmed through physical fabrication. This work represents a substantial advancement in the domain of RF filtering structures, particularly through the investigation of planar BPF. These filters are likely to impact adaptive RF technologies, such as wireless communication systems, sensor networks, and radar systems, thanks to their inherent flexibility and adaptability.

2. MICROSTRIP CIRCULAR RING RESONATOR THEORY

This research's theoretical section will detail the fundamental relationships required to calculate the critical dimensions and parameters for the proposed filter's design. The geometry of the microstrip circular ring resonator circuit is illustrated in Figure 2.

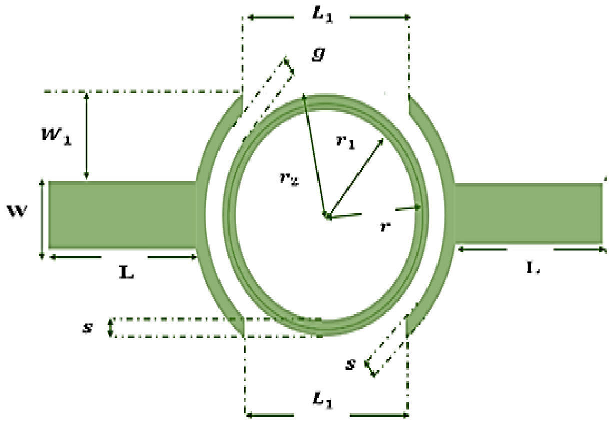

Figure 2. The geometry of the microstrip ring resonator circuit

For the PCB substrate height h, we assume the common condition w/h>1. Under this assumption, the line width w can be determined by iteratively solving the coupled (1) and (2) [25]:

$$\varepsilon_{eff} = \frac{\varepsilon_r+1}{2} + \frac{\varepsilon_r-1}{2}(1+\frac{12h}{W})^{-1/2} \quad (1)$$

$$Z_0 = \frac{120\pi}{\sqrt{\varepsilon_{eff}}[\frac{W}{h}+1.393+\frac{2}{3}ln\,(\frac{W}{h}+1.444)]} \quad (2)$$

The fundamental principle of a ring resonator is that its mean circumference (2πr) must be an integer multiple of the guided wavelength (λ_g).

$$2\pi r = n\lambda_g \quad (3)$$

The dominant mode of operation, where n=1, is typically selected. This allows for the calculation of the guided wavelength, λ_g, as (4) [25]:

$$\lambda_g = \frac{\lambda_0}{\sqrt{\varepsilon_{eff}}} = \frac{c}{f_r\sqrt{\varepsilon_{eff}}} \quad (4)$$

where c represents the speed of light, f_r is the resonant frequency of the microstrip circular ring resonator structure, and ε_{eff} is its effective permittivity.
The length, L, of the feed lines on either side of the ring is equal to:

$$L = \frac{\lambda_g}{4} \quad (5)$$

Now, combining (3) and (4), the mean radius of the ring follows as (6) [26]:

$$r = \frac{c}{2\pi f_r\sqrt{\varepsilon_{eff}}} \quad (6)$$

The inner and outer radii of the ring are set to:

$$r_1 = r - \frac{W}{2} \quad (7)$$

$$r_2 = r + \frac{W}{2} \quad (8)$$

The microstrip line width, W, for both the feed line and the ring, is determined by (1) and (2). The Table 1 shows the optimized geometric parameters for the proposed BPF.

Table 1. Values of the different parameters for the proposed BPF

Parameters	Values (mm)
W	3
W_1	4.15
L	4.85
L_1	7.3
r_1	5
r_2	5.5
g	0.5
s	0.5

3. DESIGN PROCEDURE AND RESULTS DISCUSSION

3.1. Design by advanced design system

The proposed BPF's structure is defined by a central microstrip circular ring resonator and modified microstrip lines connected to it at each end. These lines are designed to have a 50 Ω impedance. This specific configuration was optimized for simplicity, resulting in a compact size of 11.25×22.46 mm² and lower manufacturing complexity. The layout of the BPF, implemented using Agilent's advanced design system (ADS) software, is illustrated in the Figure 3. The Figure 4 illustrates the simulated S-parameters of the proposed BPF.

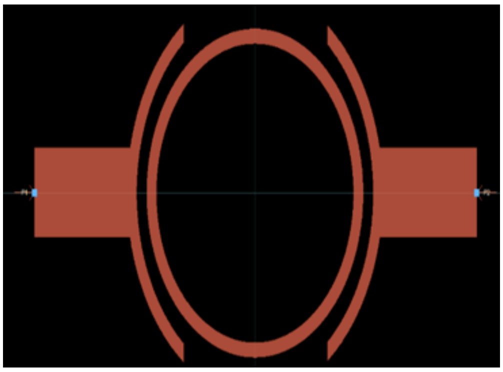

Figure 3. Layout of BPF by using ADS

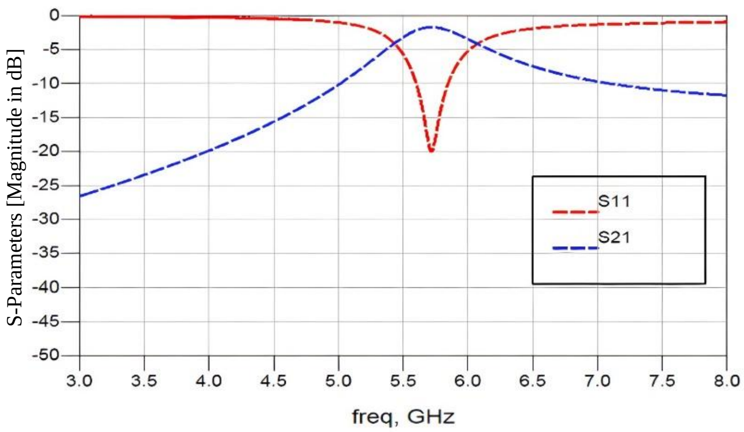

Figure 4. S-parameters versus frequency of the designed filter BPF by using ADS

Simulation results demonstrate the BPF's excellent performance at its 5.72 GHz center frequency. It exhibits a return loss of 20 dB and an insertion loss of 1.7 dB, which are desirable characteristics for a BPF. The filter's compact size and low insertion loss in the passband are complemented by a good rejection level of -20 dB at 5.72 GHz. Additionally, it achieves a total bandwidth of approximately 693 MHz.

3.2. Design by another electromagnetic solver

To validate the S-parameter results from ADS, we performed an additional simulation using a different electromagnetic solver. The layout for the BPF, designed with a different electromagnetic solver, is shown in Figure 5. The near-identical simulation results obtained from the two electromagnetic solvers, as presented in Figure 6, serve to validate the accuracy of the simulation.

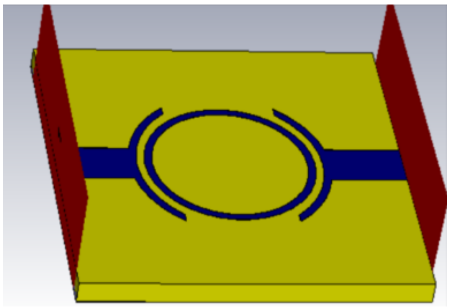

Figure 5. Layout of BPF by using another electromagnetic solver

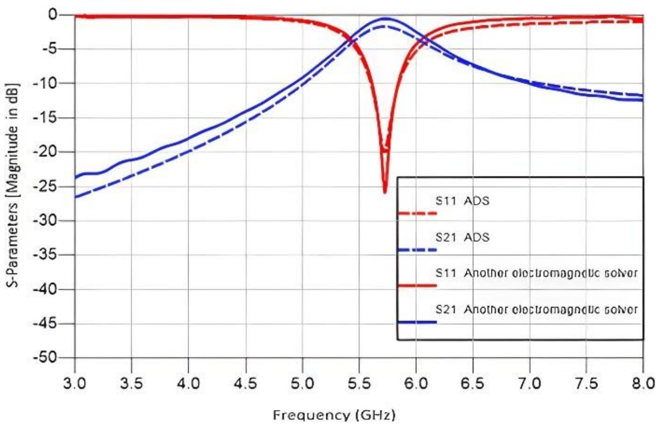

Figure 6. S-parameters versus frequency of the designed filter BPF by using another electromagnetic solver

The power flow of the proposed BPF is visualized in Figure 7, showing the behavior within the bandwidth at 5.8 GHz (Figure 7(a)) and in the rejected band at 4 GHz (Figure 7(b)). These illustrations confirm the filter's operating frequency range.

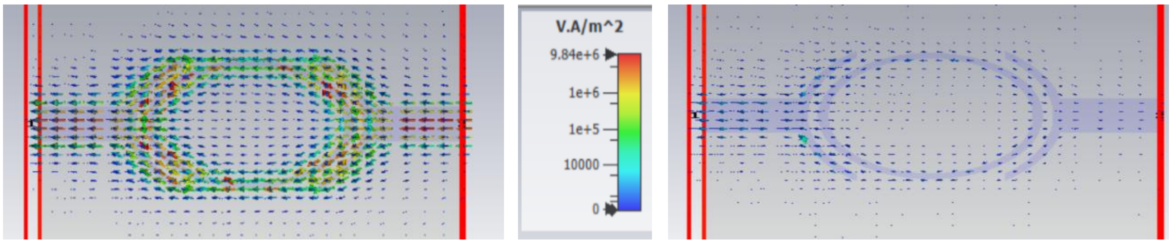

(a) (b)

Figure 7. Presents the power flow; (a) at 5.8 GHz and (b) at 4 GHz

The influence of changes in the internal radius r_1, with all other dimensions held constant, on filter performance is depicted in Figures 8 and 9. The primary goal of this analysis was to assess the filter's responsiveness to this particular design variable.

Figure 8 depicts the variations in reflection coefficients as they relate to frequency. This graph features frequency (measured in GHz) along the horizontal axis and the magnitude of the S11 and S22 parameters (expressed in dB) on the vertical axis. Each curve presented here clearly shows a minimum point, also known as a "dip," which aligns with the resonance frequency where signal reflection reaches its lowest point, indicating optimal impedance matching. In line with the transmission data, an increase in r1 results in a shift of the resonance frequency to the left, indicating lower frequencies. Additionally, as r1 grows, the reflection dip becomes more pronounced, reflecting a better impedance match at the resonance frequency.

Meanwhile, Figure 9 illustrates the variations in transmission coefficients concerning frequency. In this second graph, frequency (also in GHz) is plotted on the horizontal axis against the magnitude of the S12 and S21 parameters (in dB) on the vertical axis. For each value of r1, a distinct transmission peak is evident, marking the maximum of S21/S12 at a specific resonance frequency. As r1 increases, the resonance frequency gradually indicates resonance at the highest frequency, while the cyan curve (r1=5.25 mm) reveals resonance at the lowest frequency. Although the peak transmission amplitude shows a slight increase with r1, the overall bandwidth seems to retain a consistent width across the various r1 values.

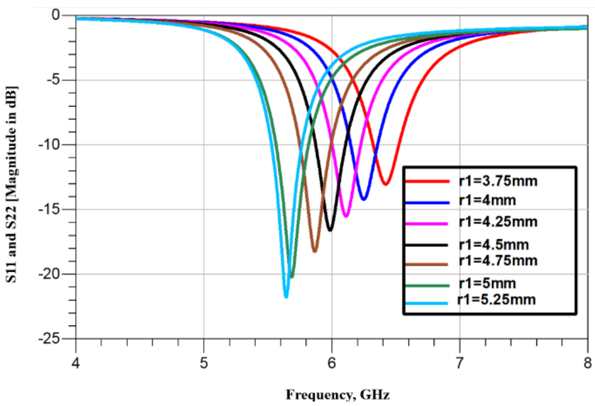

Figure 8. Variations of reflection coefficients versus frequency

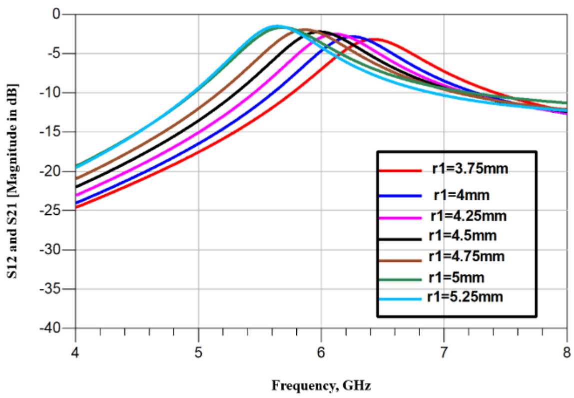

Figure 9. Variations of transmission coefficients versus frequency

Increasing the resonator's radius, r1, leads to a longer electrical length for the device, which in turn lowers its resonance frequency. This observation aligns with established resonator theory, which asserts that there is an inverse relationship between resonance frequency and the associated physical dimension, in this case, the radius. For each specific r1 value, the filter's resonance frequency, also known as the center frequency, is determined at the point of maximum transmission (S21/S12) or, alternatively, at the point of minimum reflection (S11/S22). The filter's bandwidth (BW) is generally defined by the frequency range within which the transmission (S21/S12) remains within -3 dB of its peak value. The estimated cutoff and resonance frequencies derived from the presented graphical results are compiled in Table 2.

Table 2. Tabulated cutoff and band edge frequencies for varying r_1 values

r_1 (mm)	Resonance frequency f_0 (GHz)	Low cutoff frequency f_{01} (GHz)	High cutoff frequency f_{02} (GHz)
3.75	6.42	6.02	6.86
4	6.27	5.86	6.7
4.25	6.13	5.73	6.54
4.5	5.98	5.61	6.44
4.75	5.88	5.48	6.32
5	5.63	5.17	6.1
5.25	5.61	5.3	6.09

The influence of the substrate on the characteristics of the filter was examined using simulations that included four distinct materials. The essential properties of these substrates are outlined in Table 3, while the resulting behaviors of the filters are illustrated in Figures 10 and 11. The Figure 10 illustrates variations of reflection coefficients versus frequency, the Figure 11 shows the variations of transmission coefficients versus frequency.

Table 3. properties of the substrates utilized

Substrates	Relative permittivity (ϵ_r)	Loss tangent ($\tan(\delta)$)	Thickness (H) (mm)	Copper thickness (t) (μm)
FR-4	4.4	0.025	1.6	35
RO4003C	3.38	0.0027	1.52	17.5
RO4350B	3.48	0.0037	0.508	35
RT/duroid 5880	2.2	0.0009	1.02	17.5

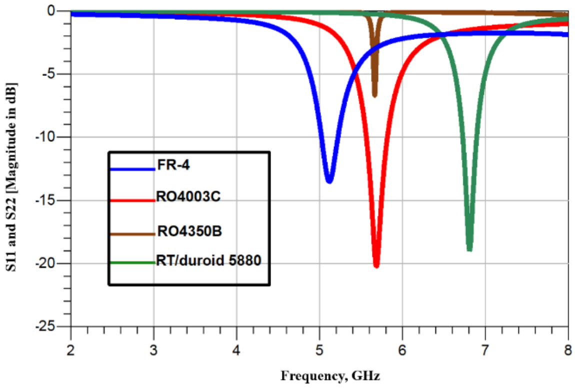

Figure 10. Variations of reflection coefficients versus frequency

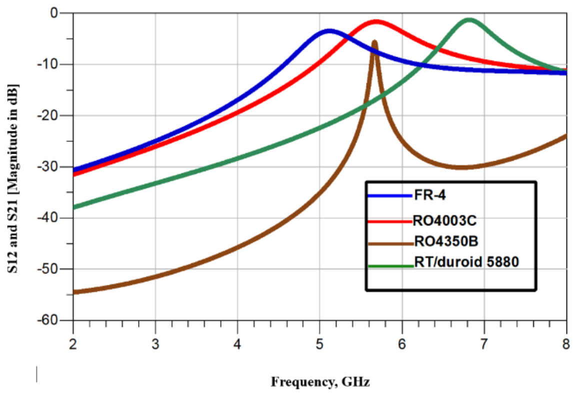

Figure 11. Variations of transmission coefficients versus frequency

Frequency response for each substrate are described below:

a. FR-4 shows the lowest resonant frequency, approximately 5.1 GHz, alongside the highest insertion loss, with a peak S21 around -5 dB, which indicates considerable signal attenuation. Its bandwidth appears to be relatively broad, but there is a notable dip at around 5.1 GHz that reaches roughly -14 dB.
b. RO4003C has a resonant frequency that is higher, around 5.6 GHz, and presents improved insertion loss, with a peak S21 nearing -2 dB. The bandwidth here seems moderate, consistent with prior discussions about this substrate. Additionally, it displays a deeper dip at approximately 5.6 GHz, reaching about -20 dB, suggesting a better impedance match compared to FR-4 at its resonant frequency.
c. RO4350B features a resonant frequency that is slightly above that of RO4003C, around 5.7 GHz, but it comes with a significantly higher insertion loss, as the peak S21 is around -8 dB or more. This substrate has a narrower bandwidth and shows a steep slope prior to the passband. It also presents a shallow dip near 5.7 GHz, only reaching about -6 dB, which points to a poor impedance match and substantial reflection.
d. RT/duroid 5880 registers the highest resonant frequency at about 6.7 GHz and the best insertion loss, with a peak S21 very close to 0 dB, signifying excellent transmission. Its passband is relatively narrow and well-defined, and it features the deepest dip around 6.7 GHz, dropping below -20 dB, which indicates outstanding impedance matching.

3.3. Fabrication and measurements

After successfully finishing the simulation and validation processes, the final design of the bandpass filter circuit was manufactured. Its physical appearance is depicted in Figure 12. The creation and printing of this filter were carried out using KLOÉ's advanced Dilase 250 direct laser writing (DLW) system. A picture of this equipment can be found in Figure 13.

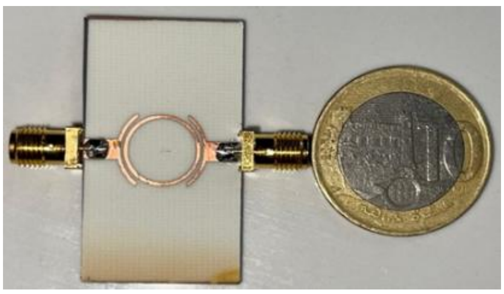

Figure 12. Photograph of the fabricated BPF

Figure 13. The dilase 250 machine from KLOÉ, a high-precision system used for DLW in photolith

This sophisticated device utilizes laser technology to inscribe or etch micro- and nanopatterns directly onto layers of photoresist, removing the need for traditional physical masks. Its applications span a variety of areas, such as integrated circuit prototyping, the creation of microelectromechanical systems (MEMS), the manufacturing of photonic devices, and various academic research and educational initiatives. The system accommodates industry-standard GDSII or Gerber file formats and includes a user interface that allows for precise adjustments of laser parameters, focal point settings, and writing speed. Common uses include the creation of microwave frequency circuits, the production of split ring resonator (SRR) and BPF, as well as conducting advanced maskless lithography experiments.

Figure 14 demonstrates a strong correlation between the performance of the measured filter and the simulated results derived from both electromagnetic solvers, confirming the design's validity. The resulting filter reaches a -3 dB cutoff frequency of 5.63 GHz and displays considerable out-of-band rejection. Its insertion loss in the passband is roughly -1.7 dB. The final design is both cost-effective and compact, making it easy to integrate into passive and active RF circuits, which enhances its suitability for a wide range of wireless communication applications.

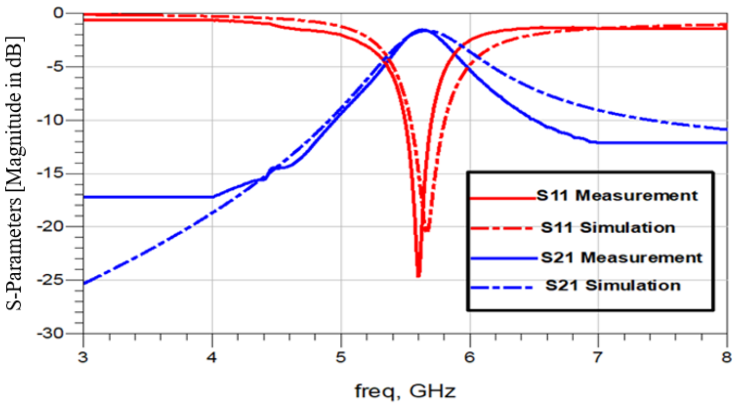

Figure 14. Simulated and physically measured S-parameters of BPF

The comparative analysis shown in Table 4 emphasizes the advantages of the proposed filter regarding its structural compactness and operational efficiency. A significant aspect that sets this work apart, as indicated in the table, is the effective physical construction and experimental testing of the prototype. In contrast to many recent studies that depend largely on theoretical simulations, this research offers empirical data that correlates well with the simulated outcomes, affirming the filter's practical dependability for high-power applications. The combination of experimental findings and up-to-date references highlights the innovation and preparedness of the design for implementation in actual wireless systems.

Table 4. Comparative study of the proposed filter and existing works

References	BW (GHz)	Filter type	Filter size (mm²)	Fabricated?
[27]	1.6-2.8	Coupled microstrip BPF	67×53	Yes
[28]	0.8-1.0	SISL BPF	39.24×23.1	No
[29]	2.0-3.0	Microstrip coupled lines BPF	80×58	No
[30]	2.0-4.0	multi-mode resonator BPF	70×36	No
This work	5.17–6.10	Microstrip filter	11.25×22.46	Yes

4. CONCLUSION

This research presents a compact band-pass filter that employs specially designed coupled ring technology. The prototype developed confirmed the expected performance, with the measured S-parameters closely aligning with the simulation outcomes. This filter functions within a bandwidth of 5.17 to 6.10 GHz, with a central frequency of 5.72 GHz, demonstrating a return loss of 20 dB and an insertion loss of 1.7 dB at that frequency. Its small size, affordability, and straightforward integration into RF circuits make this filter particularly advantageous for a range of applications. Notably, in wireless local area networks (WLANs), it improves device efficiency in the 5.8 GHz ISM band by minimizing out-of-band noise and interference, as well as in rectenna systems aimed at harvesting energy from ambient radio waves in the same frequency range.

In addition to these practical applications, the key scientific advancement of this work is the refined electromagnetic coupling mechanism of the circular rings, which offers enhanced selectivity and superior miniaturization compared to traditional designs. However, it is worth mentioning that this study was conducted under standard laboratory settings, leaving the impacts of extreme environmental conditions, such as high power levels or temperature changes on the substrate, insufficiently examined. Future investigations will aim to incorporate active tuning components, like varactor diodes, to enable frequency reconfigurability, alongside exploring multi-layer PCB technology to further improve rejection levels and overall performance.

ACKNOWLEDGMENTS

The authors thank the managers of the IETR platforms: MATRIX for fabrication and M2ARS for on-wafer characterization.

FUNDING INFORMATION

Authors state no funding involved.

AUTHOR CONTRIBUTIONS STATEMENT

This journal uses the Contributor Roles Taxonomy (CRediT) to recognize individual author contributions, reduce authorship disputes, and facilitate collaboration.

Name of Author	C	M	So	Va	Fo	I	R	D	O	E	Vi	Su	P	Fu
Soufiane El Maimouni	✓	✓	✓	✓	✓	✓		✓	✓		✓		✓	
Fouad Aytouna		✓		✓		✓	✓	✓	✓	✓		✓	✓	
Jamal Zbitou	✓		✓	✓	✓		✓		✓	✓	✓	✓	✓	
Stéphane Ginestar		✓		✓	✓		✓	✓		✓	✓			
Mohammed El Gibari	✓			✓		✓		✓	✓			✓		

C : **C**onceptualization
M : **M**ethodology
So : **So**ftware
Va : **Va**lidation
Fo : **Fo**rmal analysis
I : **I**nvestigation
R : **R**esources
D : **D**ata Curation
O : Writing - **O**riginal Draft
E : Writing - Review & **E**diting
Vi : **Vi**sualization
Su : **Su**pervision
P : **P**roject administration
Fu : **Fu**nding acquisition

CONFLICT OF INTEREST STATEMENT

Authors state no conflict of interest.

DATA AVAILABILITY

Data availability is not applicable to this paper as no new data were created or analyzed in this study.

REFERENCES

[1] F. Huang, J. Wang, J. Li, and W. Wu, "Compact microstrip wideband bandpass filter with high selectivity," *Electron. Lett.*, 52: 626-628, 2016, doi: 10.1049/el.2015.4539.
[2] Q. Liu, J. Wang, G. Zhang, L. Zhu, and W. Wu, "A New Design Approach for Balanced Bandpass Filters on Right-Angled Isosceles Triangular Patch Resonator," *IEEE Microw. Wirel. Components Lett.*, vol. 29, no. 1, pp. 5–7, Jan. 2019, doi: 10.1109/LMWC.2018.2884829.
[3] C.-Y. Chang and T. Itoh, "A modified parallel-coupled filter structure that improves the upper stopband rejection and response symmetry," *IEEE Trans. Microw. Theory Tech.*, vol. 39, no. 2, pp. 310–314, 1991, doi: 10.1109/22.102975.
[4] W. Aditomo and A. Munir, "Bandwidth enhancement of ultra-wideband microstrip bandpass filter using defected ground structure," in *2013 International Conference on QiR*, IEEE, Jun. 2013, pp. 64–67, doi: 10.1109/QiR.2013.6632538.
[5] A. Munir, R. Safitri, and M. R. Effendi, "Development of microstrip BPF using open split ring resonator with square groundplane window," in *Int. Symp. Antennas Propag. Conf. Proc.*, IEEE, Dec. 2014, pp. 49–50, doi: 10.1109/ISANP.2014.7026524.
[6] K. Salehian and M. Tayarani, "A novel SIGGW dual post band-pass filter for 5G millimeter-wave band applications with a transmission zero," *Sci. Rep.*, vol. 13, no. 1, pp. 1-9, Nov. 2023, doi: 10.1038/s41598-023-47490-1.
[7] Y.-H. Zhu, X.-Y. Fang, X. Xie, L.-L. Yang, and J.-X. Chen, "Two-Port Reflectionless Waveguide Bandpass Filter for Indoor Distribution Systems," *SSRN*, 2023, doi: 10.2139/ssrn.4635309.
[8] M. R. A. Nasser and D. Psychogiou, "Reflective and quasi-reflectionless multiband bandpass filters using multi-resonant acoustic-wave lumped-element resonators," *Int. J. Microw. Wirel. Technol.*, vol. 17, no. 2, pp. 318–330, Mar. 2025, doi:

10.1017/S1759078724001211.
[9] F. Martin, F. Falcone, J. Bonache, R. Marques, and M. Sorolla, "Miniaturized coplanar waveguide stop band filters based on multiple tuned split ring resonators," *IEEE Microw. Wirel. Components Lett.*, vol. 13, no. 12, pp. 511–513, Dec. 2003, doi: 10.1109/LMWC.2003.819964.
[10] J. B. Pendry, A. J. Holden, D. J. Robbins, and W. J. Stewart, "Magnetism from conductors and enhanced nonlinear phenomena," *IEEE Trans. Microw. Theory Tech.*, vol. 47, no. 11, pp. 2075–2084, 1999, doi: 10.1109/22.798002.
[11] B. Hasanah, F. Filiana, A. I. Ismail, A. Munir, and D. Herdiana, "Implementation of Circular Waveguide Band Pass Filter using Artificial Dielectric Resonator for Transverse Electric Propagation Mode," in *2021 IEEE Asia-Pac. Conf. Wireless Mobile (APWiMob)*, IEEE, Apr. 2021, pp. 95–98, doi: 10.1109/APWiMob51111.2021.9435255.
[12] S. Naoui, L. Latrach, and A. Gharsallah, "Equivalent circuit model of double split ring resonators," *Int. J. Microw. Opt. Technol.*, vol. 11, no. 1, pp. 1–6, 2016.
[13] J.-S. Hong and M. J. Lancaster, *Microstrip filters for RF/ Microwave applications*. New York, USA: John Wiley & Sons, Inc., 2001.
[14] H. Zhu and A. Abbosh, "Compact tunable bandpass filter with wide tuning range using ring resonator and short-ended coupled lines," *Electron. Lett.*, vol. 51, no. 7, pp. 568–570, Apr. 2015, doi: 10.1049/el.2015.0346.
[15] L.-L. Qiu and Q.-X. Chu, "Balanced Bandpass Filter Using Stub-Loaded Ring Resonator and Loaded Coupled Feed-Line," *IEEE Microw. Wirel. Components Lett.*, vol. 25, no. 10, pp. 654–656, Oct. 2015, doi: 10.1109/LMWC.2015.2463228.
[16] A. Ennajih, J. Zbitou, M. Latrach, A. Errkik, L. El Abdellaoui, and A. Tajmouati, "Dual band metamaterial printed antenna based on CSRR for RFID applications," *Int. J. Microw. Opt. Technol.*, vol. 12, no. 2, pp. 106–113, 2017.
[17] X. Y. Li and M. S. Tong, "A Bandstop Filter Based on Inverted Microstrip Gap Waveguide for Millimeter-Wave Communications," in *2022 IEEE Int. Symp. Antennas Propag. USNC-URSI Radio Sci. Meet. (AP-S/URSI)*, IEEE, Jul. 2022, pp. 549–550, doi: 10.1109/AP-S/USNC-URSI47032.2022.9886555.
[18] F. Zhu, G. Q. Luo, Z. Liao, X. W. Dai, and K. Wu, "Compact Dual-Mode Bandpass Filters Based on Half-Mode Substrate-Integrated Waveguide Cavities," *IEEE Microw. Wirel. Components Lett.*, vol. 31, no. 5, pp. 441–444, May 2021, doi: 10.1109/LMWC.2021.3066569.
[19] C. Guo, J. Li, J. Xu, and H. Li, "An X-band lightweight 3-D printed slotted circular waveguide dual-mode bandpass filter," in *2017 IEEE Int. Symp. Antennas Propag. USNC/URSI Nat. Radio Sci. Meet.*, IEEE, Jul. 2017, pp. 2645–2646, doi: 10.1109/APUSNCURSINRSM.2017.8073365.
[20] A. R. Azad and A. Mohan, "Single- and Dual-Band Bandpass Filters Using a Single Perturbed SIW Circular Cavity," *IEEE Microw. Wirel. Components Lett.*, vol. 29, no. 3, pp. 201–203, Mar. 2019, doi: 10.1109/LMWC.2019.2893379.
[21] A. Munir, Edwar, J. Haidi, Sulistyaningsih, R. S. Asthan, and A. A. Nugroho, "A Compact Narrowband Circular Waveguide Bandpass Filter with High Selectivity Incorporating Magneto-Dielectric Material," in *2025 Photonics Electromagn. Res. Symp. (PIERS) - Spring (PIERS-Spring)*, IEEE, May 2025, pp. 1–5, doi: 10.1109/PIERS-Spring66516.2025.11276746.
[22] X. Li, X. Cao, Q. Cai, Y. Zhu, Y. Qi, and J. Fan, "Dual-mode Bandpass Filter based on Circular Fractal Patch Resonator for WLAN Applications," in *2021 IEEE Int. Symp. Antennas Propag. USNC-URSI Radio Sci. Meet. (APS/URSI)*, IEEE, Dec. 2021, pp. 163–164, doi: 10.1109/APS/URSI47566.2021.9703793.
[23] Q. Liu, G. Zhang, and L. Zhu, "A Simple and General Method for Cross-Coupled Bandpass Filters Based on Circular Patch Resonator," *IEEE Trans. Microw. Theory Tech.*, vol. 71, no. 9, pp. 3991–4002, Sep. 2023, doi: 10.1109/TMTT.2023.3248165.
[24] S. AL Morabetil, M. Rifi, H. Terchoune, and J. Zbitou, "High Efficiency Rectifier Circuit For Ambient RF Energy Harvesting Applications At 5.8 Hz," in *2019 7th Mediterr. Congr. Telecommun. (CMT)*, IEEE, Oct. 2019, pp. 1–5, doi: 10.1109/CMT.2019.8931352.
[25] C. A. Balanis, *Antenna Theory: Analysis and Design*, Third Edit. Hoboken, New Jersey, USA: John Wiley & Sons, 2005.
[26] D. M. Pozar, *Microwave Engineering*. Hoboken, New Jersey, USA: John Wiley & Sons, 2005.
[27] M. F. Haider, F. You, T. Qi, C. Li, and S. Ahmad, "Co-Design of Second Harmonic-Tuned Power Amplifier and a Parallel-Coupled Stub Loaded Resonator," *IEEE Trans. Circuits Syst. II Express Briefs*, vol. 67, no. 12, pp. 3013–3017, Dec. 2020, doi: 10.1109/TCSII.2020.2991888.
[28] T. Feng, K. Ma, Y. Wang, and J. Hu, "Bandpass-Filtering Power Amplifier With Compact Size and Wideband Harmonic Suppression," *IEEE Trans. Microw. Theory Tech.*, vol. 70, no. 2, pp. 1254–1268, Feb. 2022, doi: 10.1109/TMTT.2021.3124254.
[29] M. Boumalkha, M. Lahsaini, M. El H. Archidi, and Y. Achaoui, "Design of a wideband, highly efficient FPA using an asymmetrical open-circuit coupled-lines-based filtering matching network," *AEU - Int. J. Electron. Commun.*, vol. 178, p. 155293, May 2024, doi: 10.1016/j.aeue.2024.155293.
[30] M. Boumalkha *et al.*, "Investigating broadband filtering power amplifier using multi-mode resonator-based bandpass filter," *Results Eng.*, vol. 26, pp. 1-15, Jun. 2025, doi: 10.1016/j.rineng.2025.105035.

BIOGRAPHIES OF AUTHORS

Soufiane El Maimouni was born in Ahfir, Morocco, in 1991. He received his master's degree in telecommunications from Abdelmalek Essaadi University, Tetuan, Morocco, in 2016. He is currently pursuing a Ph.D. in Electronics and Telecommunications at the National School of Applied Sciences (ENSA), Tangier, within the same university. His research is conducted at the LABTIC laboratory, where his primary interests focus on the study and design of planar filters for 5G applications. He can be contacted at email: soufiane.elmaimouni@etu.uae.ac.ma.

Pr. Fouad Aytouna was born in Beni Rzine, Morocco, in 1978. He received the Master's degree in Electronics and Telecommunications from Abdelmalek Essaadi University, Tetouan, Morocco, in 2010. He received his Ph.D. and Habilitation to Supervise Research (HDR) from Abdelmalek Essaadi University, Tetouan, Morocco, in 2017 and 2021, respectively. He is currently an Associate Professor at Abdelmalek Essaadi University, Tetouan, Morocco. His research interests include the analysis and design of planar microwave circuits. He can be contacted at email: faytouna@uae.ac.ma.

Pr. Jamal Zbitou was born in Fes, Morocco, in June 1976. He received the Ph.D. degree in electronics from Polytech of Nantes, the University of Nantes, France, in 2005. He is currently a full professor of electronics at the National School of Applied Sciences (ENSA), Tetuan, Abdelmalek Essaadi University, Morocco. He is involved in the design of hybrid, monolithic active and passive microwave electronic circuits. He is involved also in the design of rectennas, RFID tag and their applications in wireless communications, and wireless power transmission (WPT). He is the General Chair of the International Conference on Computing and Wireless Communication Systems (ICCWCS). He is the author or co-author of more than 205 Scopus-indexed scientific publications, editor of four handbooks and book, and a thesis advisor and co-advisor of 35 Ph.D. students. He can be contacted at email: j.zbitou@uae.ac.ma.

Pr. Stéphane Ginestar obtained his Ph.D. in 2009 from the Institut d'Électronique, de Microélectronique et de Nanotechnologie (IEMN). He is currently the head of the cleanroom facility in Nantes and co-head of the MATRIX platform at IETR. His main mission is to provide the institute with technological support for the development and integration of multifunctional thin-film materials—featuring tunable permittivity, piezoelectric, electromechanical, and electro-optical properties—into components and sub-components for innovative telecommunications applications within the framework of the laboratory's research projects. He can be contacted at email: stephane.ginestar@univ-nantes.fr.

Pr. Mohammed El Gibari is an associate professor at Nantes University, received his Ph.D. and HdR from Nantes University respectively in 2009 and 2025. His current research activities at the Institut d'Électronique et des Technologies du NuméRique (IETR) focus on three main areas: The first concerns the development of opto-microwave components based on thin-film polymers, with particular emphasis on microwave access for modulators and analog-to-digital converters. The second area investigates the impact of nanoparticle integration on the electro-optical properties of polymer materials. Finally, his work includes the design and fabrication of piezoelectric sensors, as well as implantable piezoresistive blood pressure sensors for medical applications. He is author and co-author of over 80 journal articles and conference papers. He can be contacted at email: mohammed.el-gibari@univ-nantes.fr.